euspen's 22nd International Conference & Exhibition, Geneva, CH, May/June 2022
www.euspen.eu

On-machine measurement cycle for the adaptive thermal error compensation of linear axes

Nico Zimmermann[1,2], Jan-Marc Kartenbender[2], Josef Mayr[1] and Konrad Wegener[2]

[1]*inspire AG, Technoparkstrasse 1, 8805 Zurich, Switzerland*
[2]*Institute of Machine Tools and Manufacturing (IWF), ETH Zürich, Leonhardstrasse 21, 8092 Zurich, Switzerland*

zimmermann@inspire.ethz.ch

Abstract
Thermal compensation strategies are relevant for precision 5-axis machine tools, because thermal errors are among the major causes for geometric inaccuracies of machined workpieces. Therefore, many different compensation strategies have been developed to consider thermal errors in the numerical control of machine tools. However, automated and efficient thermal compensation strategies for 5-axis machine tools are still an outstanding challenge in industry. The thermal adaptive learning control (TALC) overcomes this issue by combining on-machine measurements and Auto Regressive models with eXogenous inputs (ARX). This paper presents an automated on-machine measurement cycle based on a touch trigger probe and an artefact. This on-machine measurement cycle enables the application of the TALC to the thermal errors of linear axes. The measurement cycle identifies the thermal error of a linear and a rotary axis and allows the separation of the artefact-related errors. The developed artefact is integrated into the machine tool table, to realize an efficient on-machine measurement without restricting the working space. The results of the developed on-machine measurement cycle are validated using grid encoder measurements of the same thermal load cases. This comparison verifies a good consistency of both measurement methods. Furthermore, the TALC is applied to a linear axis of a 5-axis machine tool. The results show that the TALC method significantly reduces the positioning error of the considered linear axes.

On-machine measurement, thermal error, compensation, machine tool

1. Introduction

The accessible tolerances in precision manufacturing are strongly connected to the accuracy of the used machine tools (MTs). According to Mayr et al. [1] thermal errors are a main source of inaccuracies at produced workpieces. Therefore, lately model-based thermal error compensation strategies have been implemented to reduce the thermal errors of MTs. Due to the increased capability of artificial intelligence, the level of automatization of compensation strategies is further improved by introducing self-optimizing thermal error compensation models as presented by Zimmermann et al. [2]. However, the successful implementation of these thermal error compensation strategies require reliable and efficient measurement cycles as stated by Wegener et al. [3].

The commonly used measurement methods to identify the position- and time-dependent thermal errors of linear axes require specific devices such as laser interferometers or comparator systems and a time-consuming measurement setup. Blaser et al. [4] use a comparator system to characterize in detail the thermal behavior of a gantry-type linear axis considering various thermal load cases. The obtained data are then used to create a non-adaptable thermal error compensation model for the thermal positioning error of the linear axis. However, these measurement methods require expensive devices and time-consuming setups, so that they are not suitable as on-machine measurement cycle to check the current prediction accuracy of the thermal error compensation models.

Therefore, an increased number of on-machine measurement cycles, which are based on a touch trigger probe and an artefact, are introduced to measure thermal errors of linear axes. Kim and Chung [5] introduce for example an invar artefact consisting of cubes and columns to identify the thermal zero point drift the squareness errors and the positioning errors of three linear axes. Furthermore, in the case of five-axis MTs, the error separation between the rotary and linear axis becomes important. Mayer et al. [6] developed a measurement cycle to separate the thermal errors of linear and rotary axes of a 5-axis MT. However, all these measurement cycles are based on artefacts and require several artefacts in the working space. to get a complete image of the thermal behavior and distinguish the errors according to their origin.

This paper presents an on-machine measurement cycle, which is based on an artefact integrated into the notch of the machine table and a touch trigger probe, to identify the thermal errors of a linear and a rotary axis.

2. On-machine measurement cycle

This section describes the artefact and the procedure of the on-machine measurement cycle to identify the thermal errors of a linear and a rotary axis.

2.1. Artefact

The designed artefact is derived from a ball array artefact, which is presented in ISO 230-1:2012 [7] to analyse the thermal errors of linear axes. However, holes instead of spheres are chosen as features to identify the position-dependent thermal errors along the linear axis. This minimizes the space requirements in the working area of the MT and enables an integration of the artefact into a notch of the machine table as shown in Figure 1. The artefact is featured with seven holes which are irregularly distributed over the length of 320 mm to

enable the identification of periodical positioning errors as proposed by ISO 230-2:2014 [8]. The artefact is made of steel (S355 J2C) because the procedure of the measurement cycle allows a partial error separation between artefact- and machine-specific thermal errors due to the available rotary axis. A headless screw, which is in the reference hole, connects the artefact to the machine table.

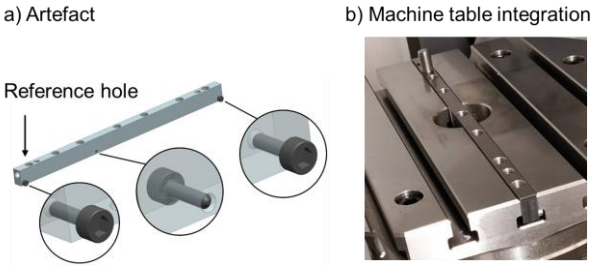

Figure 1. Designed artefact and its integration into a notch of the machine tool table

2.2. Measurement procedure

The designed artefact is suitable for identifying the position dependent thermal errors of a linear axis. Furthermore, the artefact also enables the identification of the thermal errors of a C-axis (E_{XOC}, E_{YOC}, E_{ZOT}, E_{ROT}, E_{AOC}, E_{BOC}, E_{COC}). This combination allows a separation of the artefact-related thermal error (E_{ME}) when the artefact is eccentrically fixed on the machine table due to the possible reversal measurement. As shown in Figure 2, the measurement cycle starts by measuring the position of all holes along the X-axis. Then, the C-axis is rotated by 90° and only the reference hole is measured. At the C-axis angle of 180°, the reversal measurement of the artefact is conducted at three different positions and finally the reference hole is measured at a C-axis angle of 270°. The X- and the Y-coordinate of the hole center are identified by measuring the hole on four positions and the Z-coordinate is obtained by touching the artefact in Z-direction next to the considered hole.

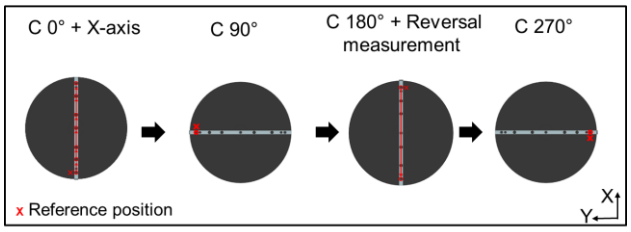

Figure 2. Measurement procedure to identify the thermal errors of X- and C-axis including the thermal error of the artefact

The mathematical model to realize the error separation consists of homogeneous transformation matrices which include the position-dependent and the position-independent thermal errors of the considered axes and the artefact. The positioning error of the linear axis and the thermal expansion of the artefact are assumed as a linear function increasing with the distance from the reference hole.

$$\underline{\underline{E}}_X(t_i,P)=\begin{bmatrix}1&0&0&E_{XX,lin}(t_i)\cdot X_P\\0&1&0&0\\0&0&1&0\\0&0&0&1\end{bmatrix} \quad (1)$$

$$\underline{\underline{E}}_C(t_i)=\begin{bmatrix}1&-E_{COC}(t_i)&E_{BOC}(t_i)&E_{XOC}(t_i)\\E_{COC}(t_i)&1&-E_{AOC}(t_i)&E_{YOC}(t_i)\\-E_{BOC}(t_i)&E_{AOC}(t_i)&1&E_{ZOT(t_i)}\\0&0&0&1\end{bmatrix} \quad (2)$$

$$\underline{\underline{E}}_T(t_i,P)=\begin{bmatrix}1&0&0&-E_{ROT}(t_i)\cdot\cos(C_P)\\0&1&0&E_{ROT}(t_i)\cdot\sin(C_p)\\0&0&1&E_{ZOT}(t_i)\\0&0&0&1\end{bmatrix} \quad (3)$$

$$\underline{\underline{E}}_{art}(t,P)=\begin{bmatrix}1&0&0&E_{ME,lin}(t_i)\cdot X_{art}\cdot\cos(C_P)\\0&1&0&E_{ME},lin(t_i)\cdot X_{art}\cdot sin(C_P)\\0&0&1&0\\0&0&0&1\end{bmatrix} \quad (4)$$

The kinematic chain of the analysed machine tool is modelled by using the presented homogeneous transformation matrices. Finally, the thermal errors are identified by solving the resulting system of equations using the Jacobian matrix $\underline{\underline{J}}$.

$$\underline{E}=\underline{\underline{J}}^{-1}\cdot\underline{\Delta P} \quad (5)$$

The vector $\underline{E}$ contains all considered thermal errors and the vector $\underline{\Delta P}$ summarizes the differences between the current and the reference hole positions.

3. Evaluation of the measurement cycle

The performance of the developed measurement cycle is evaluated by applying it to a five-axis machine tool with the following kinematic chain according to ISO 10791-1:2015 [9]:
V [w – C2' – A' – X' – b – Y – Z – C1 – t].

In the following, the accuracy, the dominant thermal errors of the considered linear axis, the repeatability and the error separation capability of the new on-machine measurement cycle are evaluated.

3.1. Cross grid comparison

The accuracy of the on-machine measurement cycle is analysed by comparing the identified thermal positioning error to the measurement results of a commonly used grid encoder (Heidenhain KGM 200). This comparison encompasses thermal WarmCold load cases of the X-axis with different feed rates as presented by Blaser et al. [4]. During the WarmCold load case, the X-axis oscillates over the whole distance of travel for the first four hours and the thermal errors are measured every five minutes. In the cool-down phase, which also lasts four hours, the X-axis is not moved between the measurements.

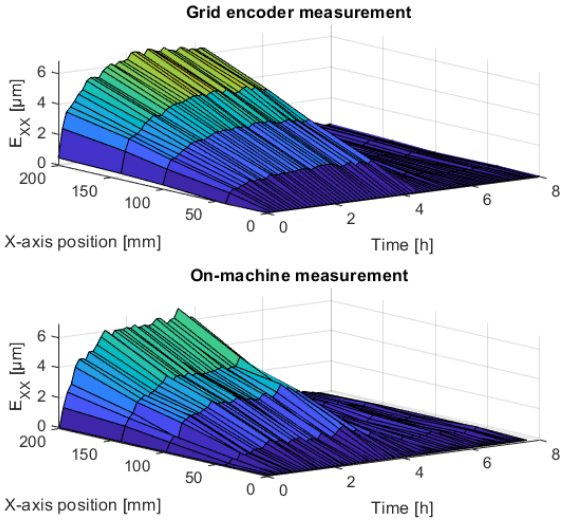

Figure 3. Positioning errors of the X-axis for a thermal WarmCold load case of the X-axis with a feed rate of 30 m/min identified by the grid encoder (top) and the on-machine measurement cycle (bottom).

Figure 3 illustrates the comparison between the positioning error of the X-axis measured by the on-machine measurement

and the grid encoder. The results indicate a good agreement between the two measurement methods, although the measurements are conducted in a not air-conditioned workshop, which means different environmental conditions. This demonstrates that the new on-machine measurement cycle correctly identifies the thermal positioning errors of linear axes without requiring a complex measurement cycle.

3.2. Analysis of the dominant thermal errors

In this section, the position-dependent thermal errors of the considered linear axis are analysed. Figure 4 presents the thermal zero-point drift and the corresponding translational thermal component errors at the different hole positions. The results depict, that the positioning error is the most dominant component error and a neglection of the thermal components errors E_{YX} and E_{ZX} in the mathematical model of the measurement cycle is reasonable.

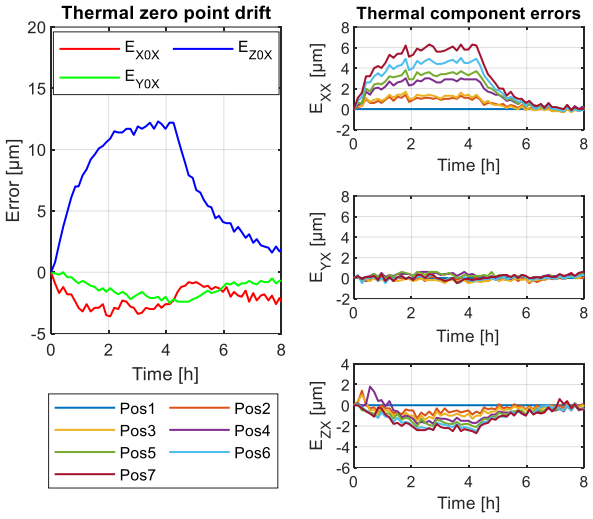

Figure 4. Thermal zero-point drift and the position-dependent component errors of the X-axis for a thermal WarmCold load case of the X-axis with a feed rate of 30 m/min.

Furthermore, the location dependence of the thermal positioning error is evaluated more in detail because the assumption of a linear increase of the positioning error with the distance of travel allows a reduction of the number of measurement positions. Therefore, Figure 5 shows the deviation between the measured and the linearly increasing positioning.

$$E_{XX}(t,x) = E_{XX,lin}(t) \cdot x \qquad (6)$$

The maximum deviation at the considered measurement positions is approximately 0.6 µm for a WarmCold load case with a feed rate of 30 m/min, which is shown in Figure 5. Furthermore, the same analysis is also conducted for a thermal MultiRange load case. This demonstrates the impact of different oscillation locations on the resulting thermal positioning error as shown by Blaser et al. [4]. It encompasses the oscillation at three different regions of the overall distance of travel of the X-axis. The maximum difference between the measured and the approximated linearly increasing positioning error is 0.4 µm for a MultiRange load case with a feed rate of 15 m/min. Consequently, the positioning error can be approximated as linear function depending on the distance of travel. This reduces the resulting measurement and modelling effort because only one thermal error compensation model, which predicts the slope of the function, is required.

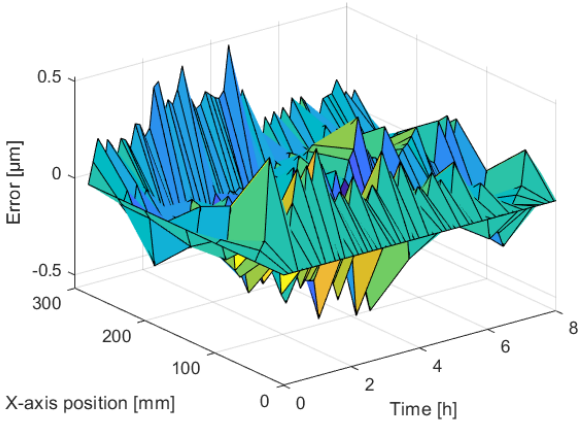

Figure 5. Difference between the approximated linearly increasing and the measured thermal positioning error E_{XX} for a thermal WarmCold load case with a feed rate of 30 m/min.

3.3. Repeatability

The repeatability of the measurement cycle is analysed by repeating it 100 times in a row. A high-pass filter is applied to the experimental data in order to eliminate the long-term thermal drifts due to the variation of the environmental temperature. The resulting measurement repeatability (k=2) is maximum 0.4 µm for the translational errors (E_{X0C}, E_{Y0C}, E_{Z0T} E_{R0T}), 1.8 µm/m for the positioning error $E_{XX,lin}$, 1.6 µm/m for the rotational errors (E_{A0C}, E_{B0C}, E_{C0C}) and 1.6 µm/m for the thermal error of the artefact $E_{ME,lin}$.

3.4. Error separation

The error separation between the thermal errors of the MT and the thermal elongation of the artefact is especially relevant because no material with a small thermal expansion coefficient is chosen to realize an affordable artefact. Figure 6 shows the machine- and artefact-related errors obtained from the on-machine measurement cycle for a thermal WarmCold load case of the C-axis with a rotational speed of 120 rpm. The temperature of the machine table rises due to the rotation of the C-axis results in a significant thermal elongation of the artefact, which is correctly separated from the considered machine-specific errors.

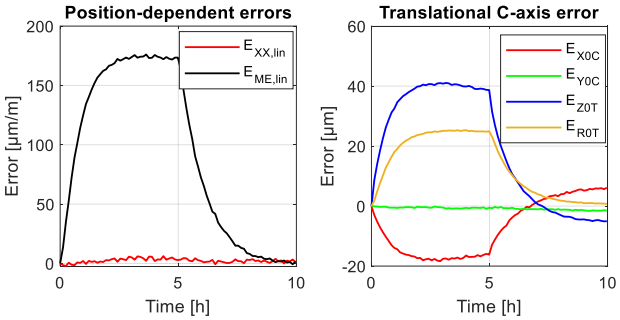

Figure 6. Separated artefact- and machine-specific thermal errors for a thermal WarmCold load case of the C-axis with a rotational speed of 120 rpm.

4. Compensation experiment

The new on-machine measurement cycle enables an efficient application of self-optimizing thermal error compensation models to reduce the thermal errors of linear and a rotary axis. The self-optimizing thermal error compensation models presented by Zimmermann et al. [2,10,11] include an adaptive selection of the optimal model inputs and on-demand triggered on-machine measurements to check the current accuracy of the

compensation results. Figure 7 summarizes the applied self-optimizing thermal error compensation strategy.

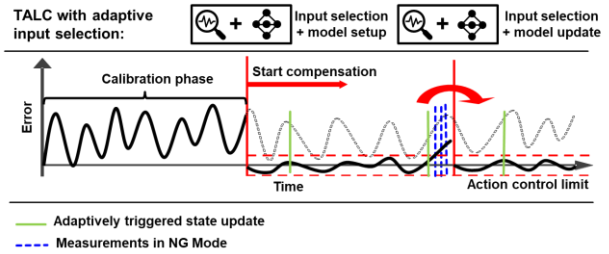

Figure 7. Concept of the TALC in combination with the adaptive input selection and the autonomously triggered on-machine measurements adapted from [11].

In total 29 sensors measure the temperatures of the different machine tool components and the environment. The concept of the self-optimizing thermal error compensation models is applied to compensate the thermal errors of an X- and a C-axis resulting from a randomly generated speed profile of the X-axis. Figure 8 illustrates the used speed profile.

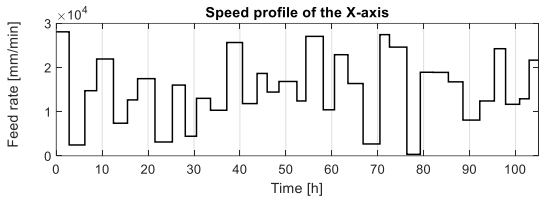

Figure 8. Speed profile of the X-axis over 105 hours.

Figure 9 presents the corresponding compensation results for the thermal errors E_{XX}, E_{X0C} and E_{Z0T}. The root-mean-square error of the thermal positioning error E_{XX} is reduced by 87%. Furthermore, root-mean-square error of the translational errors of the C-axis E_{X0C} and E_{Z0T} are reduced by 86% and respectively 79%. Consequently, the on-machine measurement cycle enables in combination with the self-optimizing thermal error compensation models an efficient reduction of the thermal errors.

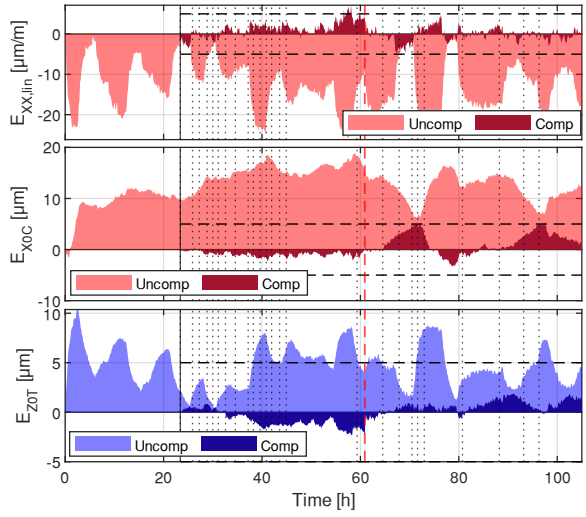

Figure 9. Uncompensated and compensated thermal errors E_{XX}, E_{X0C} and E_{Z0T} for the thermal load case shown in Fig. 8. The black vertical line shows the time of the model setup and the black doted lines represent the autonomously triggered state updates to check an exceedance of the action control limit (ACL), which is represented by the black dashed horizontal lines. The red dashed vertical line indicates an exceedance of the ACL of any error.

5. Conclusion and Outlook

The introduced artefact-based on-machine measurement cycle provides an efficient identification of the thermal errors of a linear axis and a rotary axis without requiring a complex measurement setup. The on-machine measurement cycle enables an error separation between the artefact- and the machine related thermal positioning error of a linear axis if a rotary axis is available. The conducted evaluation using a grid encoder demonstrate the accuracy of the new measurement cycle. The conducted experiments illustrate, that the positioning error is the dominant thermal component error of the considered linear axis. Furthermore, the results show that the thermal positioning error can be approximated by a linear position-dependant function with a time-dependent slope, which reduces the measurement and modelling effort significantly. The combination of the developed on-machine measurement cycle and self-optimizing thermal error compensation models reduces for example the positioning error of a linear axis by 87%.

Future research concentrates on extending the developed measurement cycle on a second linear axis, which requires a thermally stable reference length as an additional component to realize an error separation between the considered axes.

References

[1] Mayr, J., Jedrzejewski, J., Uhlmann, E., Alkan Donmez, M., Knapp, W., Härtig, F., Wendt, K., Moriwaki, T., Shore, P., Schmitt, R., Brecher, C., Würz, T., Wegener, K., 2012, Thermal issues in machine tools, CIRP Annals - Manufacturing Technology, 61/2:771–791.

[2] Zimmermann, N., Breu, M., Mayr, J., Wegener, K., 2021, Autonomously triggered model updates for self-learning thermal error compensation, CIRP Annals, 00:4–7.

[3] Wegener, K., Weikert, S., Mayr, J., 2016, Age of compensation – challenge and chance for machine tool industry, International Journal of Automation Technology, 10/4:609–623.

[4] Blaser, P., Hauschel, C., Rüttimann, R., Hernández-Becerro, P., Mayr, J., Wegener, K., 2019, Thermal characterization and modelling of a gantry-type machine tool linear axis, European Society for Precision Engineering and Nanotechnology, Conference Proceedings - 19th International Conference and Exhibition, EUSPEN 2019, /June:166–169.

[5] Kim, K. D., Chung, S. C., 2003, On-machine inspection system: Accuracy improvement using an artifact, Journal of Manufacturing Systems, 22/4:299–308.

[6] Mayer, J. R. R., 2012, Five-axis machine tool calibration by probing a scale enriched reconfigurable uncalibrated master balls artefact, CIRP Annals - Manufacturing Technology, 61/1:515–518.

[7] ISO 230-1:2012, Test code for machine tools — Part 1: Geometric accuracy of machines under no-load or quasi-static conditions, International Organization for Standardization ISO, Geneva, Switzerland.

[8] ISO 230-1:2014, Test code for machine tools — Part 2: Determination of accuracy and repeatability of positioning of numerically controlled axes, International Organization for Standardization ISO, Geneva, Switzerland.

[9] ISO 10791-1:2015, Test Conditions for Machining Centres – Part 1: Geometric tests for machines with horizontal spindle (horizontal Z-axis), International Organization for Standardization ISO,Geneva, Switzerland.

[10] Zimmermann, N., Lang, S., Blaser, P., Mayr, J., 2020, Adaptive input selection for thermal error compensation models, CIRP Annals, 69/1.

[11] Zimmermann, N., Büchi, T., Mayr, J., Wegener, K., 2022, Self-optimizing thermal error compensation models with adaptive inputs using Group-LASSO for ARX-models, 50th SME North American Manufacturing Research Conference (under review).